Long-term safety and absorption assessment of a novel bioresorbable nitrided iron scaffold in porcine coronary artery

Jian-Feng Zheng [a,1], Zi-Wei Xi [a,1], Yang Li [a], Jia-Nan Li [g], Hong Qiu [a,**], Xiao-Ying Hu [a], Tong Luo [a], Chao Wu [a], Xin Wang [b], Lai-Feng Song [c], Li Li [c], Hai-Ping Qi [d], Gui Zhang [d], Li Qin [d], Wan-Qian Zhang [d], Xiao-Li Shi [e], Shu-Han Wang [f], De-Yuan Zhang [d], Bo Xu [a], Run-Lin Gao [a,*]

[a] Department of Cardiology, Fuwai Hospital, National Center for Cardiovascular Diseases, Chinese Academy of Medical Sciences and Peking Union Medical College, Beijing, China
[b] Beijing Key Laboratory of Pre-clinical Research and Evaluation for Cardiovascular Implant Materials, Animal Experimental Center, Fuwai Hospital, National Center for Cardiovascular Diseases, Chinese Academy of Medical Sciences and Peking Union Medical College, Beijing, China
[c] Department of Pathology, Fuwai Hospital, National Center for Cardiovascular Diseases, Chinese Academy of Medical Sciences and Peking Union Medical College, Beijing, China
[d] R&D Center, Biotyx Medical (Shenzhen) Co. Ltd., Shenzhen, China
[e] National and Local Joint Engineering Laboratory of Interventional Medical Biotechnology and System, Lifetech Scientific (Shenzhen) Co. Ltd., Shenzhen, China
[f] Shen Zhen Testing Center of Medical Devices, Shenzhen, China
[g] Department of Cardiology and Macrovascular Disease, Beijing Tiantan Hospital, Capital Medical University, Beijing, China

ARTICLE INFO

ABSTRACT

This study aimed to investigate the long-term biocompatibility, safety, and degradation of the ultrathin nitrided iron bioresorbable scaffold (BRS) in vivo, encompassing the whole process of bioresorption in porcine coronary arteries. Fifty-two nitrided iron scaffolds (strut thickness of 70 μm) and 28 Vision Co–Cr stents were randomly implanted into coronary arteries of healthy mini-swine. The efficacy and safety of the nitrided iron scaffold were comparable with those of the Vision stent within 52 weeks after implantation. In addition, the long-term biocompatibility, safety, and bioresorption of the nitrided iron scaffold were evaluated by coronary angiography, optical coherence tomography, micro-computed tomography, scanning electron microscopy, energy dispersive spectrometry and histopathological evaluations at 4, 12, 26, 52 weeks and even at 7 years after implantation. In particular, a large number of struts were almost completely absorbed in situ at 7 years follow-up, which were first illustrated in this study. The lymphatic drainage pathway might serve as the potential clearance way of iron and its corrosion products.

1. Introduction

Bioresorbable scaffold (BRS) has been developed to overcome limitations of drug-eluting stent (DES), which are designed to set the vessel free from a permanent metallic stent and provide similar temporary performance to DES before safe and sufficient absorption, with the expectation of restoring vascular vasomotion and preventing the detrimental long-term effects of permanent metallic stents [1,2].

The poly (L-lactic acid)-based Absorb BVS (Abbott Vascular, Santa Clara, CA, USA) was the first commercialized scaffold as a biodegradable

Table 1
Groups and follow-up times of experiment.

Follow-up	Nitrided iron scaffold (n = 52)	Vision stent (n = 28)	Methods
4 W	8	8	A, B, E, F, G
12 W	8	6	A, B, F, G
26 W	8	6	A, B, F, G
52 W	8	8	A, B, F, G
2.5 Y	8	/	A, B, F, G
4.5 Y	6	/	A, B, D, F, G
7 Y	6	/	A, B, C, D, F, G, H

Note: A = quantitative coronary angiography; B = optical coherence tomography; C = intravenous ultrasound; D = micro–computed tomography; E = scanning electron microscopy; F = histology; G = immunohistochemistry; H = energy dispersive spectrometry; W = weeks; Y = years.

coronary stent. Late adverse clinical events especially device thrombosis of Absorb BVS were identified among randomized trials and observational registration studies in long term follow-up [3,4], leading to the subsequent withdrawal of these devices. Absorbable metal scaffolds such as magnesium scaffold and iron scaffold constitute attractive candidates to BRS as they conform more to the procedure and performance of permanent DES. Favorable clinical outcomes of magnesium BRS Magmaris (Biotronik) were observed during two-year follow-up with a low adverse events rate including scaffold thrombosis [5]. However, real-world evidence with lager sample size and longer follow-up is still required to support their safety and efficacy. As to the iron material serving as another alternative for BRS, primary studies have shown its safety, efficacy, and good mechanical performance, but also exposed some drawbacks such as the slow degradation and long bioresorption period [6,7]. Furthermore, there is no report to show the complete

absorption of iron BRS in vivo.

Previous animal experiments by Waksman [6] and Peuster [8] had proved the safety, lack of toxicity, and efficacy of pure iron scaffolds during short and long-term follow-up. The short-term safety and efficacy of the bioresorbable nitrided iron coronary scaffold, developed by Lifetech Scientific (Shenzhen, Guangdong, China), were also confirmed in previous research [9]. In this study, we firstly report the long-term findings and complete degradation and bioresorption process of this nitrided iron scaffold, which is the platform of sirolimus-eluting iron bioresorbable coronary scaffold (IBS).

2. Materials and methods

2.1. Materials

The bioresorbable nitrided iron coronary scaffold has been reported previously [9,10]. It consists overall of a balloon-expandable bioresorbable metal scaffold made of nitrided iron (Fe alloyed with ~0.05 wt% N), manufactured by Lifetech Scientific (Shenzhen, Guangdong, China), as shown in Supplementary Fig. S1. Advantages for these scaffolds included: (1) ultrathin strut (70 μm); (2) high strength comparable to Co–Cr stent; (3) good ductility (anti-fracture); and (4) higher corrosion rate in comparison to the pure iron scaffold, as reported in a previous study [11]. The control group used the Vision stent (Co–Cr alloy, strut thickness 81 μm, Abbott Vascular, Santa Clara, CA, USA) which was purchased from the market with the same specification to iron scaffold (3.0 × 18 mm).

2.2. Animal models and implantation

This study was approved by the Institutional Animal Ethics
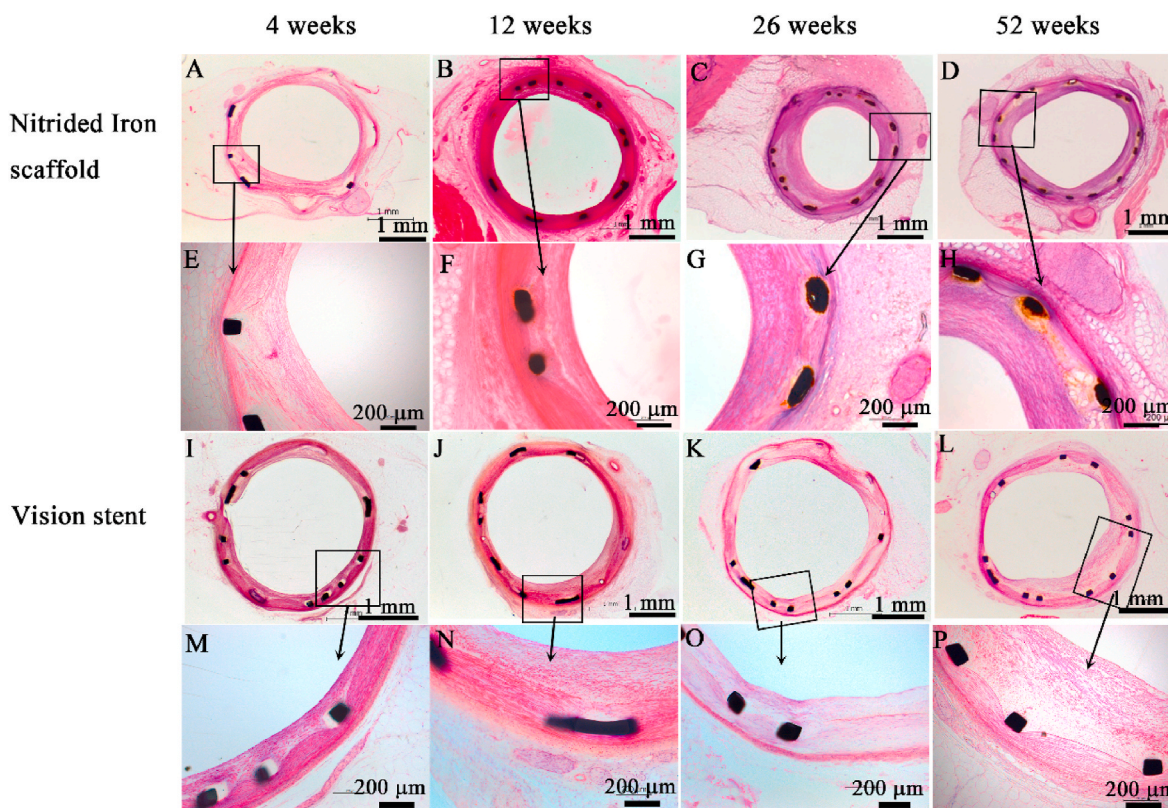
Fig. 1. Representative histological images of nitrided iron scaffold and Vision stent in porcine coronary artery (HE staining). No destruction or loss of vascular lamina was observed in either group. All cell response except macrophages and plasma cells were not significantly different between groups throughout 52 weeks follow up. Nitrided iron scaffold: (A) 4 weeks, (B) 12 weeks, (C) 26 weeks, and (D) 52 weeks (× 40); (E–H) an enlargement of the rectangular area in (A–D) (× 100). Vision stent: (I) 4 weeks, (J) 12 weeks, (K) 26 weeks, and (L) 52 weeks (× 40); (M − P) an enlargement of the rectangular area in (I–L) (× 100).

Table 2
Comparison of histopathological measurement between nitrided iron scaffold and Vision stent at 4, 12, 26, 52 weeks.

	4 weeks			12 weeks			26 weeks			52 weeks		
	Nitrided iron scaffold (N = 8)	Vision stent (N = 8)	P	Nitrided iron scaffold (N = 8)	Vision stent (N = 6)	P	Nitrided iron scaffold (N = 8)	Vision stent (N = 6)	P	Nitrided iron scaffold (N = 8)	Vision stent (N = 6)	P
LA (mm^2)	3.15 ± 1.10	3.84 ± 1.76	0.363	3.11 ± 1.24	3.62 ± 1.08	0.426	2.00 ± 1.37	2.05 ± 1.57	0.960	2.95 ± 1.70	3.16 ± 1.50	0.816
IEMA (mm^2)	5.71 ± 1.50	6.89 ± 1.73	0.167	5.62 ± 1.14	5.46 ± 0.92	0.782	5.16 ± 0.79	5.10 ± 0.41	0.855	5.41 ± 0.40	5.59 ± 0.59	0.519
EEMA (mm^2)	9.53 ± 2.63	10.85 ± 2.09	0.288	7.48 ± 1.55	6.40 ± 0.95	0.135	6.90 ± 1.10	7.10 ± 0.59	0.674	5.94 ± 0.44	6.75 ± 0.95	0.099
MeNT (mm)	0.46 ± 0.17	0.45 ± 0.18	0.878	0.35 ± 0.18	0.24 ± 0.18	0.270	0.53 ± 0.31	0.64 ± 0.23	0.461	0.21 ± 0.17	0.24 ± 0.26	0.798
NA (mm^2)	2.55 ± 0.91	3.04 ± 1.15	0.360	2.51 ± 1.27	1.84 ± 1.34	0.367	3.15 ± 1.44	3.05 ± 1.44	0.898	2.45 ± 1.65	2.44 ± 1.82	0.986
AS (%)	44.5 ± 11.4	46.0 ± 18.0	0.845	44.6 ± 19.7	32.4 ± 22.8	0.320	61.4 ± 25.5	60.5 ± 29.0	0.953	45.6 ± 29.3	42.1 ± 28.0	0.826
Stent restenosis (n/%)	0	0	–	0	0	–	3/38%	2/33%	–	2/25%	1/17%	–

LA = Lumen area; IEMA = Internal elastic membrane area; EEMA = External elastic membrane area; MeNT = Mean Neointima thickness; NA = Neointima area; AS(%) = percentage of area stenosis; Stent restenosis is defined as AS ≥ 70% in cross section.

Committee of Fuwai Hospital. Experiments were conducted using forty healthy mini-swines, 8–9 months old, weighing 25–35 kg (Da Shuo Biotechnology Co., Ltd, Cheng Du, China). The mini-swines were randomly divided into nitrided iron scaffold group (n = 52) or Vision stent group (n = 28) (Table 1). One day before the implantation procedure, the pigs received a loading dose of 300 mg aspirin and 300 mg clopidogrel. Anesthesia was performed by injecting ketamine (25 mg/kg) and diazepam (1 mg/kg) intramuscularly with limb lead ECG monitoring, after which the animals were intubated and supported with mechanical ventilation. Coronary angiography was performed through the femoral artery. Animals were then implanted with experimental nitrided iron scaffold or control Vision stent in the left anterior descending (LAD) and right coronary artery (RCA) under the guidance of coronary angiography; all scaffolds/stents were implanted with a 1.1–1.2:1 of stent/artery (diameter) ratio. The left circumflex artery (LCX) was used if the LAD or RCA was not suitable for scaffold/stent implantation. The procedural details of coronary angiography and scaffold/stent implantation were described previously [12]. After implantation, 100 mg aspirin and 75 mg clopidogrel were given daily for three months, then 100 mg aspirin per day was given through the respective follow-up time period until the animals were sacrificed.

2.3. In vivo imaging assessments

Intravascular images were acquired using coronary angiography (Allura Xper FD20, Philips Medical Systems, Best, the Netherlands), optical coherence tomographic (OCT) imaging (M2 and C7 XR, Light Lab Imaging, St. Jude Medical, Westford, Massachusetts) and intravascular ultrasound (IVUS) imaging (Boston Scientific Corp/SCIMED, Minneapolis, MN, USA). Quantitative coronary angiography (QCA) analysis (Inturis; Philips Medical Systems) was conducted to confirm the size and morphology of vessels and blood flow. An OCT or IVUS catheter was positioned in the distal end of the scaffolded or stented segment with a 0.014-inch guidewire through a 6-F guiding catheter. The scaffolded or stented vessel segment was scanned using an OCT catheter with automatic pull-back at 20 mm/s and an IVUS catheter with automatic pull-back at 0.5 mm/s. IVUS analysis was performed only in the seven years follow-up group.

2.4. Ex vivo assessments

After in vivo imaging observation, the animals were sacrificed by injection of potassium chloride. A thoracotomy was performed to harvest the heart and other organs according to the methods described previously [9]. The tissues adjacent to the scaffolded/stented arteries, myocardium as well as liver, spleen, lung, and kidney were rapidly harvested and immersed into a 4% formaldehyde solution for fixation, followed by paraffin embedding, slicing, and HE staining and iron staining (Prussian blue method) [9].

The scaffold/stent segments were cut carefully into sections as illustrated in Supplementary Fig. S2, and the sample preparation methods and assessments were described as following: (a) Blank vessels taken from the proximal and distal (section AB and FG in Supplementary Fig. S2) were immersed into a 4% formaldehyde solution for fixation, followed by paraffin embedding, slicing, and HE staining. (b) The scaffold/stent segments including proximal and distal edges (sections BC, DE and EF in Supplementary Fig. S2) were immersed in the 10% formalin for fixing, then dehydration gradient, vitrification and resin embedding in a conventional way [13]. After Harris hematoxylin-eosin (HE) staining, the scaffold/stent segment (sections C, D and E in Supplementary Fig. S2) were observed for histopathology and vessel histomorphometric measurement. All segments of scaffolded/stented coronary arteries were processed histologically for semiquantitative evaluation of the tissue reaction and biological effect by using scoring system according to ISO standard 10,993–6:2016 [14] and improved criteria of degradation and phagocytosis which applied values instead of plus signs [15]. The histologic features were divided as cell type/response, fibrosis, neovascularization, degradation and phagocytosis. Tissue reactions to implants were scored semi-quantitatively according to the following criteria [14,15](The criteria was shown in Supplementary Table S1). Furthermore, parts of resin embedded sections of scaffold crossing-sections were prepared to analysis of element composition and distribution around the scaffold struts using a scanning electron microscope (SEM, JSM-6510, JEOL, Japan) equipped with an energy-dispersive spectrometer (EDS, Oxford Inca Energy 350; Oxford Instruments, United Kingdom). In addition, scaffold/stent segments (section CD in Supplementary Fig. S2) were fixed by 10% formalin for 24–48 h at room temperature, subsequently removed the struts from vessel by manually (for Vision stent) or chemically [11](for nitrided iron scaffold), then dehydrated in gradient alcohol and embedded in paraffin. Finally, 4–5 μm paraffin-embedded sections were prepared using a rotary microtome (LEICA RM2235, Germany) and stained using HE, ET + VG, Masson, or immunohistochemical stainings including endothelial nitric oxide synthase (eNOS), smooth muscle α-actin (SMA) and CD31 stainings. The chemical dissolving method of nitrided iron struts was briefly described as follows: nitrided iron scaffold with the

Table 3

Tissue reaction of nitrided iron scaffolds and Vison stents at 4, 12, 26, 52 weeks.

Cell type/response		4 weeks			12 weeks			26 weeks			52 weeks		
		Nitrided iron scaffold (N = 8)	Vision stent (N = 6)	p	Nitrided iron scaffold (N = 8)	Vision stent (N = 6)	p	Nitrided iron scaffold (N = 8)	Vision stent (N = 6)	p	Nitrided iron scaffold (N = 8)	Vision stent (N = 6)	p
	Polymorphonuclear cells	1 (1)	1 (1)	0.709	0 (1)	0 (1)	0.781	0 (1)	0 (1)	0.825	0 (0)	0 (0)	0.403
	Lymphocytes	0 (0)	0 (0)	0.945	1 (1)	0 (0)	0.739	1 (0)	1 (1)	0.116	1 (1)	0 (1)	0.127
	Plasma cells	0 (0)	0 (0)	1	0 (0)	0 (0)	1	0 (0)	0 (0)	0.016	0 (0)	0 (0)	0.016
	Macrophages	0 (1)	0 (0)	0.001	1 (1)	0 (0)	<0.001	2 (2)	0 (0)	<0.001	3 (1)	0 (0)	<0.001
	Giant cells	0 (0)	0 (0)	1	0 (0)	0 (0)	1	0 (0)	0 (0)	0.077	0 (0)	0 (0)	0.384
	Necrosis	0 (0)	0 (0)	1	0 (0)	0 (0)	1	0 (0)	0 (0)	1	0 (0)	0 (0)	1
Fibrosis		0 (0)	0 (0)	1	0 (0)	0 (0)	1	0 (0)	0 (0)	1	0 (0)	0 (0)	1
Neovascularization		0 (0)	0 (0)	1	0 (0)	0 (0)	1	0 (1)	0 (0)	<0.001	0 (1)	0 (0)	0.001
Degradation		0 (1)	0 (0)	<0.001	1 (0)	0 (0)	<0.001	2 (1)	0 (0)	<0.001	2 (1)	0 (0)	<0.001
Phagocytosis		0 (0)	0 (0)	0.009	0 (1)	0 (0)	0.001	1 (1)	0 (0)	<0.001	2 (1.5)	0 (0)	<0.001

Note: the meaning of score was concluded in Supplementary Table 1.

scaffolded vessel was soaked in a mixture acid solution consisting of 80 ml ethyl alcohol, 10 ml 40% formaldehyde, 5 ml glacial acetic acid, and 5 ml 65% nitric acid for 24 h at room temperature to dissolve the strut [11]. This method had been verified to be effective in removing the residual iron struts and no adverse influence on the fixed tissue/cells. Then the samples underwent dehydration with 100% ethanol for 1 h, and then vitrified with xylol for 30 min and paraffin embedding for 30 min. (c) At 4 weeks follow-up time point, two scaffold/stent segments of nitrided iron scaffold or Vison stent (section CD in Supplementary Fig. S2) were picked out randomly, and carefully cut along the vertical line into two symmetrical parts and immediately fixed using a 2.5% glutar-aldehyde solution at 4 °C, respectively. After dehydrated in gradient alcohol and critical point drying, the segments were gold-sputtered for scanning electron microscopy (JSM-6510, JEOL, Akishima, Japan) to assess endothelialization.

In addition, scaffolded vessel segments with nitrided iron scaffold after 4.5 years and 7 years implantation were undergone micro-computed tomography (Micro-CT) (Skyscan 1172, Bruker, Kontich, Belgium) before cutting off to examine degradation of the nitrided iron scaffold, which can evaluate the corrosion degree and distinguish between iron and iron corrosion products.

3. Statistical analysis

Continuous variables were described as mean ± standard deviation (SD) or median and interquartile ranges (IQR) according to the normality of data distribution tested by the Shapiro-Wilk test. Categorical variables were summarized by frequency and percentage. The Student's t-test and Mann-Whitney U test was used to compare continuous variables. The Pearson chi-square or Fisher's exact test for categorical variables. A value of $p < 0.05$ was considered statistically significant. Statistical analysis was done with SPSS 11.0 (IBM, Armonk, New York, USA).

4. Results

4.1. General condition and follow-up findings

All scaffolds/stents were successfully implanted into porcine coronary arteries. There were no complications such as acute thrombosis, dissection, malapposition, or collapse during the procedures identified by immediate angiography. All animals remained healthy during the scheduled follow-up period, except one pig in the control group died from pneumonia at 52 weeks after stents implantation. In both group, no stent migration, thrombosis or aneurysms was found in coronary angiography and no evidence of myocardial infarction, epicardial hemorrhage, or other obvious abnormalities along the coronary arteries was found in heart gross histological examination during the follow-up.

4.2. Efficacy, biocompatibility and safety

The scaffolds and stents were fully expanded and showed no malapposition, collapse or thrombosis at follow-up in both groups by QCA and OCT examinations. The typical QCA images at each time point were shown in Supplementary Fig. S3. The representative histopathological images of nitrided iron scaffold and Vision stent were shown in Fig. 1, demonstrating no destruction or loss of vascular lamina in either group. Histopathological measurement outcomes were presented in Table 2. No significant difference was found in lumen area (LA), neointimal area (NA), internal elastic membrane area (IEMA), and percentage of area stenosis (AS) between the two groups.

There was no significant difference in endothelialization between nitrided iron scaffold and Vision stent during follow-up, as shown in Supplementary Fig. S4, the endothelialization rate reached 95% at 4 weeks after implantation. And the endothelial cells (ECs) function restored at 12 weeks after implantation (Supplementary Fig. S5) in the

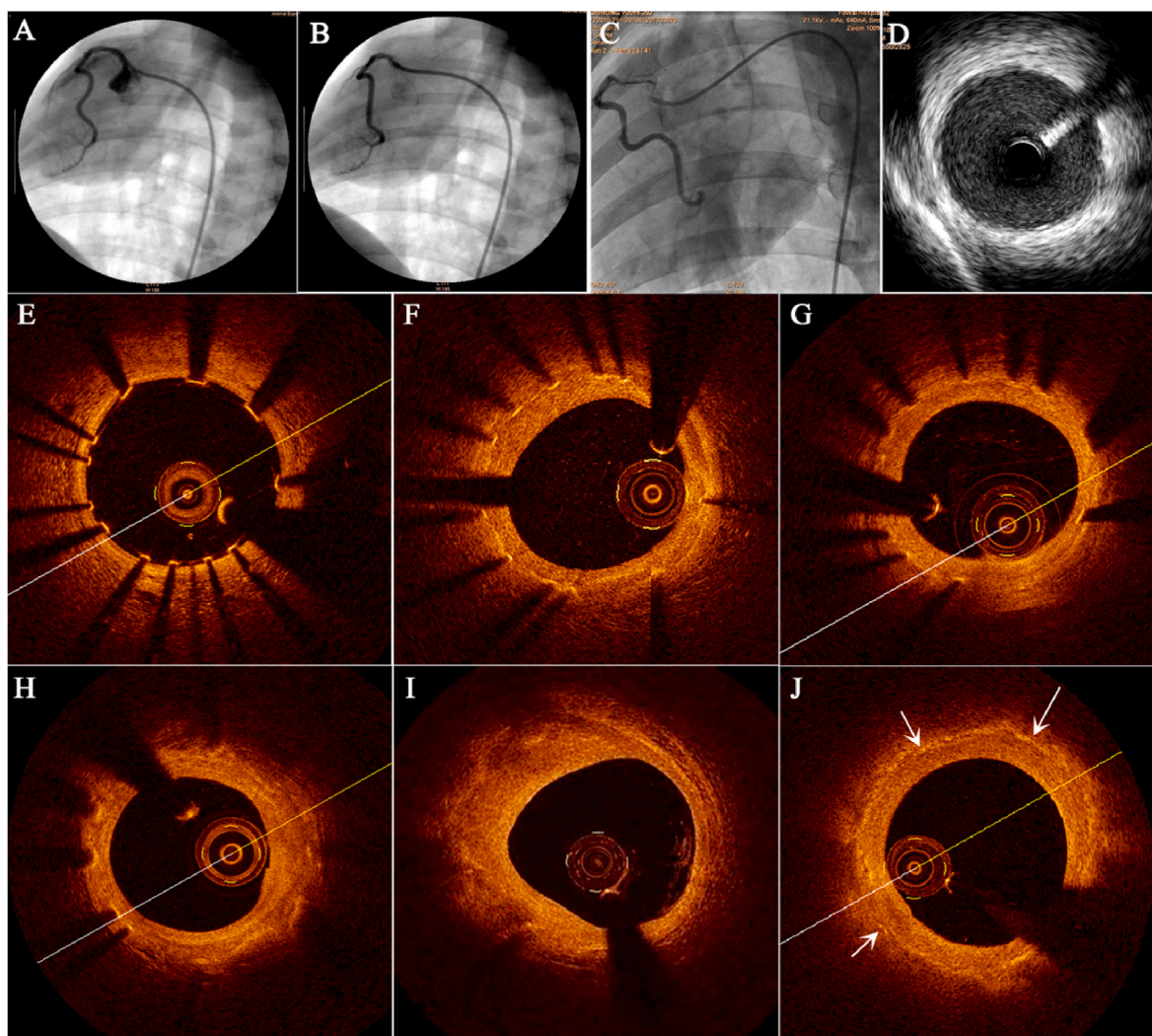**Fig. 2. Imaging manifestations of nitrided iron scaffold after implantation.** The typical QCA images of a 3.0 × 18 mm nitrided iron scaffold was implanted in porcine right coronary artery: (A) pre-implantation, (B) post-implantation and (C) at 7 years after implantation. The angiography showed that the scaffolded artery had restored to bend shape at 7 year after implantation. (D) Intravascular ultrasound image at 7 years after implantation showed uniform strong echoes in the blood vessel wall, and no ultrasound attenuation was detected. There was no any trail of the struts, indicating the scaffolds were almost completely degraded. Furthermore, each OCT frame represented the observations at different time points, revealing the process of corrosion and absorption of nitrided iron scaffold as well: (E) post implantation, (F) at 4 weeks, all scaffold structure remained complete; (G) at 52 weeks, small part of struts was corroded; (H) at 2.5 years, part of struts was corroded; (I) at 4.5 years, struts were partially corroded; and (J) at 7 years, struts were almost completely corroded and corrosion products were bioabsorbed in situ.

nitrided iron scaffold group. The neointima proliferation and scaffold/stent restenosis rates were comparable between the two groups as shown in Table 2.

The tissue reaction of nitrided iron scaffolds and Vison stents were presented in Table 3. All cell response except macrophages and plasma cell were not significantly different between groups throughout 52 weeks follow up. The fibrosis was not significantly different. Moreover, the degradation and phagocytosis of nitrided iron scaffold were obviously increase compared to Vision scaffold at all follow-up time points, and the neovascularization was visibly increased from 26 weeks follow-up as well, shown in Supplementary Fig. S6. The role of macrophages were of phagocytosis and clearance of material particles from the degradation of the scaffolds.

Iron staining in major organ tissues except spleen at 52 weeks after implantation were negative in both nitrided iron scaffold and Vision stent groups (Supplementary Fig. S7). And histopathological analysis of HE staining in major organs showed no obvious abnormality and pathological changes in both groups (Supplementary Fig. S8).

4.3. Degradation and bioresorption

The results of OCT showed that the scaffold structure remained complete at 4 weeks, corrosion was distinctly found in part of the scaffold struts at 52 weeks. The struts continued to corrode over time, until no obvious bright spot can be seen in the scaffolded vessel at 7 years, which indicated that the scaffold had been almost completely corroded (Fig. 2). Similar scaffold degradation process was also demonstrated by IVUS, micro-CT, and histopathological examination (Fig. 3, Fig. 4) at 7 years. The mass loss of iron at 7 years assessed by micro-CT was 95 ± 3% (n = 6).

After scaffold was almost completely bioabsorbed in situ, the results of QCA, OCT, and IVUS showed that the bend and structure of scaffolded artery were generally restored to its original state (Fig. 2). Histopathological examination indicated that the space of corroded scaffold struts was replaced by normal tissue, as shown in Fig. 4. This result was further confirmed by iron staining and SEM results (Fig. 5). The results of immunohistochemical tests showed that the scaffolded vessel at 7 years after implantation of nitrided iron scaffold in porcine coronary artery had structurally completed intima, media and adventitia, further
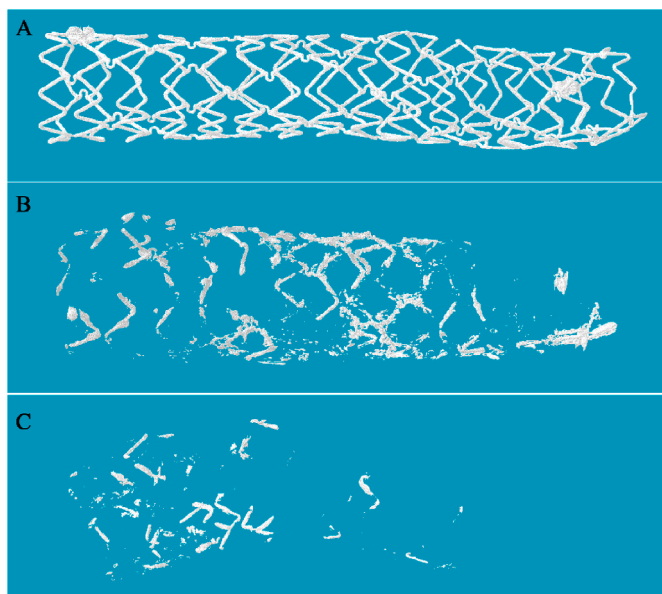
Fig. 3. Representative 3D micro-computed tomography images of the nitrided iron scaffold after implantation in the porcine coronary artery. (A) at 0 days, the scaffold showed integrity; (B) at 4.5 years, most of the struts were incomplete, indicating that the scaffold had been partially corroded; and (C) at 7 years, only a small quantity of struts were observed, indicating the scaffold had been almost completely corroded.

corroborated that the vasculature was restored to normal without residual iron corrosion products influencing the morphology and function of the neointima (Fig. 6 and Supplementary Fig. S9). EDS analyses on the surface indicated that the C element was found instead of the iron element in the original position of the iron strut, indicating that the iron was almost completely bioabsorbed in situ with tissue regeneration

within the original strut footprint (Fig. 5).

After the scaffold being corroded, the corrosion products were dispersed to the vascular adventitia, which was apparent under the IVUS examination (Fig. 2). A small quantity of iron was also found at the edge of the tissue by EDS, indicating that iron corrosion products in the form of hemosiderin had been transferred by macrophages to the adventitia of blood vessels (Fig. 5). Histopathological examination at 4.5 years showed that the iron corrosion products were engulfed by macrophages and began to migrate to the vascular adventitia. And at 7 years, there were only a small quantity of corrosion products can be observed in the vascular adventitia (Fig. 4). The mediastinal lymph node image by iron staining in the pig at 7 years after implantation of nitrided iron scaffold in coronary artery revealed residual iron corrosion products, as shown in Fig. 7, which might indicate the drainage pathway of the corroded products of the nitrided iron scaffold.

5. Discussion

This study firstly evaluated the long-term efficacy, biocompatibility, safety, and degradation of the novel nitrided iron scaffold in a porcine coronary artery model. The salient findings of this study could be summarized as follows: (1) The efficacy of the nitrided iron scaffold was comparable with that of the Vision stent by QCA, OCT, and histopathologic examinations. The nitrided iron scaffold provided sufficient vascular scaffolding within 52 weeks after implantation. (2) The biocompatibility and safety of the nitrided iron scaffold, including neointimal growth and endothelialization, were similar to that of the Vision stent at follow-up. Both groups showed complete endothelialization at 4 weeks and no adverse events were observed. There was also no local or systematic toxicity in either group. (3) The corrosion and bioresorption of the nitrided iron scaffold were assessed via intravascular images, Micro-CT, EDS, histopathological and immunohistochemical assessments, which showed that the nitrided iron scaffold struts were almost completely absorbed in situ and the structure of scaffolded vessels was recovered at 7 years follow-up. The lymphatic
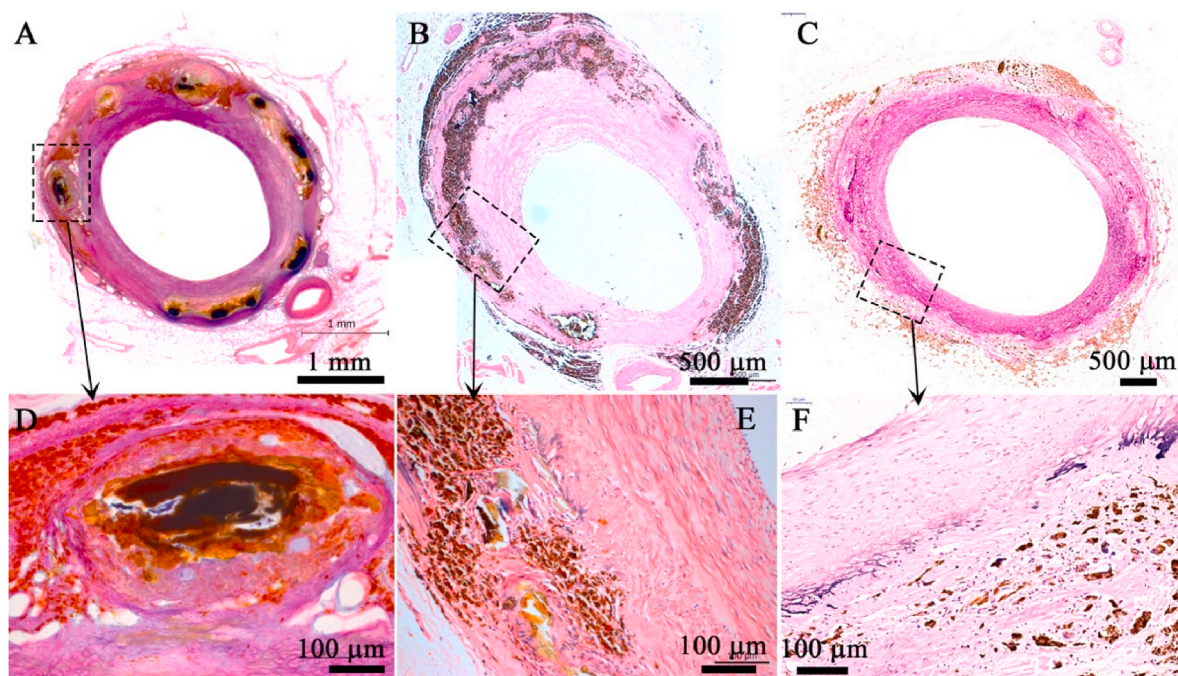

Fig. 4. Representative long-term histological images of nitrided iron scaffold in porcine coronary artery (HE staining). HE staining images at: (A) (D) 2.5 years, the scaffold was partially corroded, and there were significant granulomatous reactions with hemosiderin laden macrophages and neovascularization; (B) (E) 4.5 years, most iron struts were completely corroded, and the iron corrosion products were engulfed by macrophages and began to migrate to the vascular adventitia; (C) (F) 7 years, the iron struts were almost completely bioabsorbed in situ, and only a small quantity of corrosion products was observed in the vascular adventitia, and the space of corroded scaffold was repaired by normal tissue.
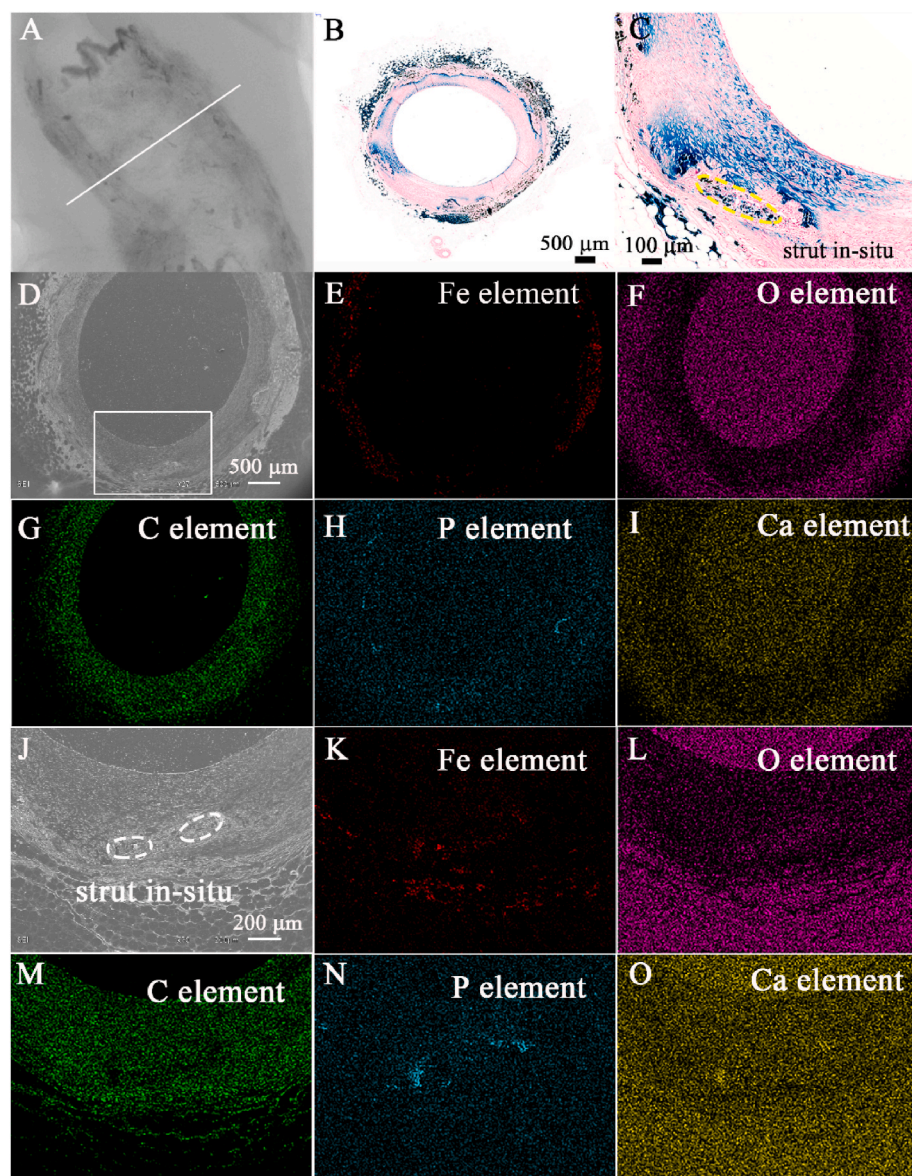
Fig. 5. Complete absorption of nitrided iron scaffold. (A) 2D micro-computed tomography image of the nitrided iron scaffold at 7 years after implantation in the porcine coronary artery, iron strut were almost completely corroded; (B) iron staining of the white line indicated area in (A); (C) magnified view of a strut in-situ and surrounding tissue; only small quantity of iron element was observed at the strut in-situ, iron element diffused into vessel. (D) scanning electron microscopic image of the white line indicated area in (A); (E)–(I) energy dispersive spectrometry (EDS) images of (D); (J) a magnified image of the rectangular area in (D); (K)–(O) EDS images of (J), small amount of Fe element was present in the outer membrane, and there were very small amounts Fe element in the margin of the strut in-situ.

drainage pathway might serve as the potential clearance route for iron and its corrosion products.

The nitrided iron scaffold used in this study, treated by surface modification technique of plasma nitriding [10], has better radial strength and corrosion rate, and a thinner stent strut thickness than pure iron stent. Previously, this novel nitrided iron scaffold showed similar efficacy, biocompatibility, and safety as the cobalt-chromium Vision stent at 28 days after implantation in a pig model by Wu et al. [9]. However, the studies were limited by lack of longer-term data to ascertain absorption period, efficacy, and safety. Therefore, the present study was the first to systematically assess the long-term biocompatibility and safety of the nitrided iron scaffold, encompassing the entire period of its bioresorption.

The present study shows that the nitrided iron scaffold is biocompatible and safe for implantation in the coronary arteries of pigs. At 52 weeks after scaffold/stent implantation, there were no significant differences in neointimal hyperplasia and area stenosis between the nitrided iron scaffold and the Vision stent as confirmed by imaging examinations, histomorphometry, and immunohistochemical investigations. Furthermore, there are no late acquired stent malapposition that might occur with traditional degradable scaffolds.

The thinner struts of the nitrided iron scaffold might contribute to lower rates of adverse events to some degree. Prior studies have shown that stent thickness is associated with in-stent restenosis, neointimal coverage, and thrombogenicity [16].

The ideal BRS could provide temporary mechanical support for vessel until endothelialization and complete vascular remodeling were achieved. Beyond this time, the stents could become the nidus for chronic inflammation and late stent thrombosis [17,18]. In this study 7 years after implantation, almost all corrosion products were bioresorbed and struts in-situ were filled with tissue. Histopathological and immunohistochemical assessments confirmed that the corroded iron scaffold did not cause iron overload or deposition of iron in organs and tissues. Iron staining in the spleen was positive in both groups indicating that it was not specific, and might be caused by the phagocytosis of senescent red blood cells and the release of iron from hemoglobin.

The iron-based scaffold can be truly completely absorbed in situ, which is different with the magnesium scaffold that leaves calcium phosphate in tissue [19–21]. The difference can be explained by the Solubility Product Constants (Ksp) of the corrosion products [22–24], as shown in Supplementary Fig. S10. Interestingly, the mediastinal lymph nodes of the pig in this study showed residual iron elements. To our
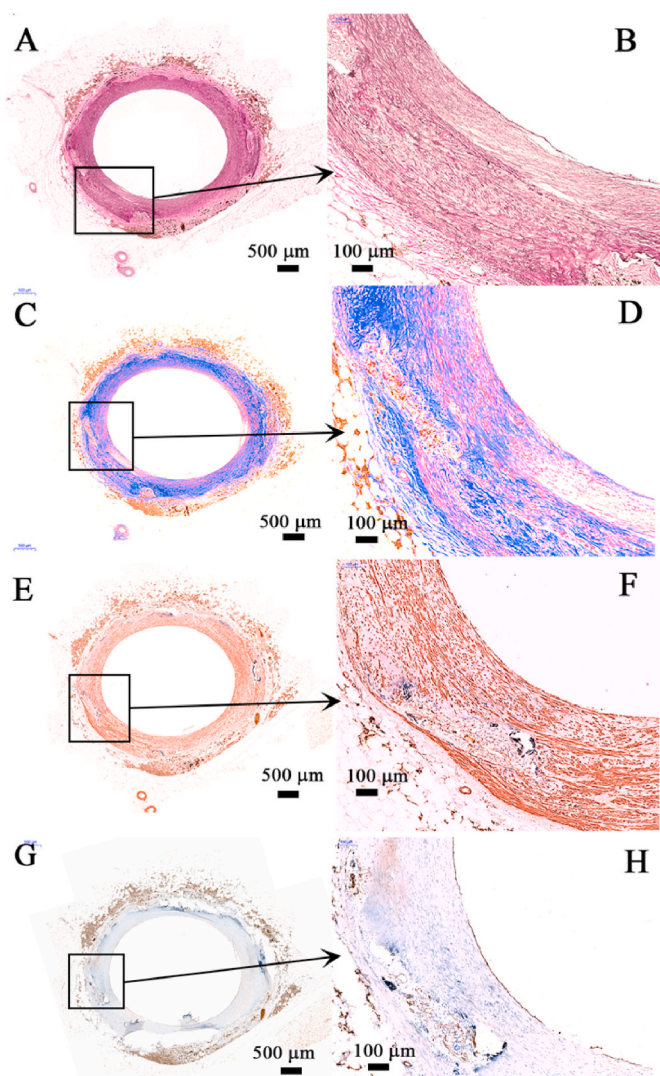
Fig. 6. Images of vascular immunohistochemical examinations of nitrided iron scaffold after 7 years implantation in porcine coronary artery. (A & B) Elastic fiber staining analysis showed that a small amount of the original inner and outer elastic plates of blood vessels remained on the vessel wall, and there was no continuous inner and outer elastic plates in the scaffold segment of the blood vessel; (C & D) Masson tricolor staining found a large number of possible smooth muscle cells (red) but only small quantity of collagen fibers (green) in neointima, which was similar to the normal vascular media; (E & F) Further immunohistochemical staining (SMA staining) confirmed that the red in Figures C and D were the smooth muscle cells and a large amount of collagen in the neointima smooth muscle cells, they were the important part of the vascular media; (G & H) On the surface of the vessel lumens, a layer of functionally mature endothelial cells could also be seen (CD31 staining). Those results showed structurally complete intima, media and adventitia were restored. (For interpretation of the references to color in this figure legend, the reader is referred to the Web version of this article.)

knowledge, the lymphatic vessel is a unidirectional absorptive vessel that transports interstitial fluid, immune cells, and macromolecules to the lymphatic nodes and returns them to the blood vessels in the circulatory system [25]. Superparamagnetic iron oxide particles have been used as tracers and probes to map lymphatic drainage pathways [26,27]. As early as 2001 and 2006 Peuster and his research team reported that clearance of the corrosion product of the iron scaffold might take place via the lymphatic circulation [7,8]. The present study supported Peuster's assumption by providing an image to show the lymphatic drainage route. A few soluble iron ions were absorbed into the blood flow, while

most of the solid corrosion products of iron were devoured by inflammatory cells like macrophages or neutrophils, and transferred to hemosiderin in adventitia by macrophages, finally to the lymph system and then to spleen by circulatory system.

There are some limitations to this study. Firstly, although the animal model in this study is the most common experimental model, no animal models represent the complex conditions of coronary artery disease in humans for which scaffolds are implanted. Secondly, the animal individual differences in the outcome could not be well distinguished between experimental and control scaffold/stent groups. In addition, although complete bioresorption time appears to occur by 5–7 years post-implantation in a healthy porcine coronary artery, there is still room for further improvement of the nitrided iron scaffold. For example, to further shorten complete bioresorption time might be achieved via nitriding technology and be combined with biodegradable polymer to prepare metal-polymer composite scaffolds [12,28–32]. Newer iron-based bioresorbable scaffolds may hold promise among BRS. In such a series of studies of new-generation biodegradable coronary scaffolds, the present publication affords an important insight about the in vivo corrosion of iron in mammals for an examined time as long as 7 years.

6. Conclusions

Taken together, the present animal study based on the porcine coronary artery model suggests that the bioresorbable 70 μm nitrided iron scaffold can be successfully implanted; it is effective and safe in comparison with the standard bare metal stent; and can be corroded and bioresorbed completely in situ with good long-term biocompatibility. The nitrided iron scaffold is promising to be an alternative to permanent stents or to be a platform of bioresorbable drug-eluting scaffold.

Subject terms

Translational Studies, Iron, Bioresorbable scaffold

Author disclosure

R. L. Gao and H. Qiu received institutional research grants from Lifetech Scientific (Shenzhen) Co. Ltd. and BiotyxMedical (Shenzhen) Co. Ltd. Shenzhen, China. H. P. Qi, L. Qin, W. Q. Zhang, G. Zhang and D. Y. Zhang are employees of BiotyxMedical (Shenzhen) Co. Ltd. X. L. Shi is employee of Lifetech Scientific (Shenzhen) Co. Ltd. All other authors have no relationships relevant to the contents of this paper to disclose.

Declaration of interest

R. L. Gao and H. Qiu received institutional research grants from Lifetech Scientific (Shenzhen) Co. Ltd. and BiotyxMedical (Shenzhen) Co. Ltd., Shenzhen, China. H. P. Qi, L. Qin, W. Q. Zhang, G. Zhang and D. Y. Zhang are employees of BiotyxMedical (Shenzhen) Co. Ltd.. X. L. Shi is employee of Lifetech Scientific (Shenzhen) Co. Ltd.. All other authors have no relationships relevant to the contents of this paper to disclose.

CRediT authorship contribution statement

Jian-Feng Zheng: conceived the study. **Zi-Wei Xi:** conceived the study. **Yang Li:** conceived the study. **Jia-Nan Li:** conceived the study. **Hong Qiu:** conceived the study, and. **Xiao-Ying Hu:** performed the experiments. **Tong Luo:** performed the experiments. **Chao Wu:** performed the experiments. **Xin Wang:** performed the experiments. **Lai-Feng Song:** performed the experiments. **Li Li:** performed the experiments, and. **Hai-Ping Qi:** Formal analysis, analyzed the data. **Gui Zhang:** Formal analysis, analyzed the data. **Li Qin:** Formal analysis, analyzed the data. **Wan-Qian Zhang:** Formal analysis, analyzed the data. **Xiao-Li Shi:** Formal analysis, analyzed the data. **De-Yuan Zhang:**
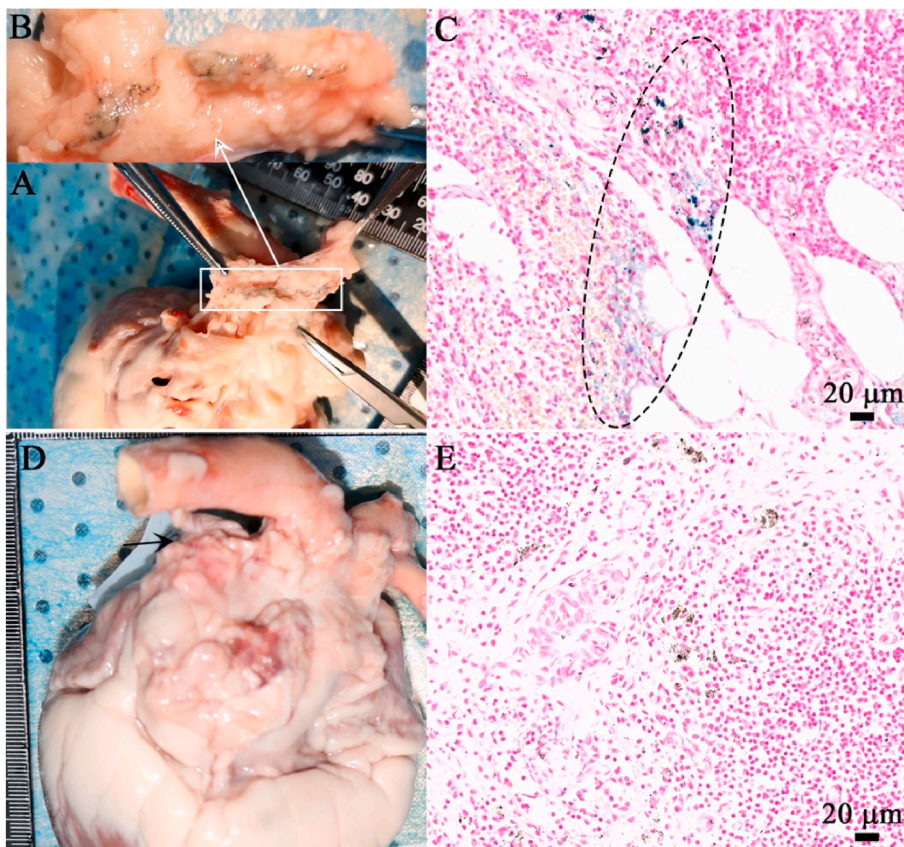
Fig. 7. The mediastinal lymph nodes image and its iron staining. (A) (B) The mediastinal lymph node was taken from the pig at 7 years after implantation of nitrided iron scaffold in coronary artery, a yellow-brown stripe indicating residue iron corrosion products could be seen within the area of white line; (C) iron staining showing the particles of iron in blue; (D) (E) The mediastinal lymph node taken from the pig that did not implant the nitrided iron scaffold, no iron element was observed. (For interpretation of the references to color in this figure legend, the reader is referred to the Web version of this article.)

Appendix A. Supplementary data

Supplementary data to this article can be found online at https://doi.org/10.1016/j.bioactmat.2022.01.005.

References

[1] H. Jinnouchi, S. Torii, A. Sakamoto, F.D. Kolodgie, R. Virmani, A.V. Finn, Fully bioresorbable vascular scaffolds: lessons learned and future directions, Nat. Rev. Cardiol. 16 (2019) 286–304.

[2] J. Iqbal, Y. Onuma, J. Ormiston, A. Abizaid, R. Waksman, P. Serruys, Bioresorbable scaffolds: rationale, current status, challenges, and future, Eur. Heart J. 35 (2014) 765–776.

[3] Z.A. Ali, P.W. Serruys, T. Kimura, R. Gao, S.G. Ellis, D.J. Kereiakes, Y. Onuma, C. Simonton, Z. Zhang, G.W. Stone, 2-year outcomes with the absorb bioresorbable scaffold for treatment of coronary artery disease: a systematic review and meta-analysis of seven randomised trials with an individual patient data substudy, Lancet 390 (2017) 760–772.

[4] T. Toyota, T. Morimoto, H. Shiomi, Y. Yoshikawa, H. Yaku, Y. Yamashita, T. Kimura, Very late scaffold thrombosis of bioresorbable vascular scaffold: systematic review and a meta-analysis, JACC Cardiovasc. Interv. 10 (2017) 27–37.

[5] M. Haude, H. Ince, S. Kische, A. Abizaid, R. Tolg, P. Alves Lemos, N.M. Van Mieghem, S. Verheye, C. von Birgelen, E.H. Christiansen, W. Wijns, H.M. Garcia-Garcia, R. Waksman, Sustained safety and clinical performance of a drug-eluting absorbable metal scaffold up to 24 months: pooled outcomes of biosolve-ii and biosolve-iii, EuroIntervention 13 (2017) 432–439.

[6] R. Waksman, R. Pakala, R. Baffour, R. Seabron, D. Hellinga, F.O. Tio, Short-term effects of biocorrodible iron stents in porcine coronary arteries, J. Intervent. Cardiol. 21 (2008) 15–20.

[7] M. Peuster, P. Wohlsein, M. Brugmann, M. Ehlerding, K. Seidler, C. Fink, H. Brauer, A. Fischer, G. Hausdorf, A novel approach to temporary stenting: degradable cardiovascular stents produced from corrodible metal-results 6-18 months after implantation into New Zealand white rabbits, Heart 86 (2001) 563–569.

[8] M. Peuster, C. Hesse, T. Schloo, C. Fink, P. Beerbaum, C. von Schnakenburg, Long-term biocompatibility of a corrodible peripheral iron stent in the porcine descending aorta, Biomaterials 27 (2006) 4955–4962.

[9] C. Wu, H. Qiu, X.Y. Hu, Y.M. Ruan, Y. Tian, Y. Chu, X.L. Xu, L. Xu, Y. Tang, R. L. Gao, Short-term safety and efficacy of the biodegradable iron stent in mini-swine coronary arteries, Chin. Med. J. 126 (2013) 4752–4757.

[10] W. Lin, G. Zhang, P. Cao, D. Zhang, Y. Zheng, R. Wu, L. Qin, G. Wang, T. Wen, Cytotoxicity and its test methodology for a bioabsorbable nitrided iron stent, J. Biomed. Mater. Res. B Appl. Biomater. 103 (2015) 764–776.

[11] W. Lin, L. Qin, H. Qi, D. Zhang, G. Zhang, R. Gao, H. Qiu, Y. Xia, P. Cao, X. Wang, W. Zheng, Long-term in vivo corrosion behavior, biocompatibility and bioresorption mechanism of a bioresorbable nitrided iron scaffold, Acta Biomater. 54 (2017) 454–468.

[12] J.F. Zheng, H. Qiu, Y. Tian, X.Y. Hu, T. Luo, C. Wu, Y. Tian, Y. Tang, L.F. Song, L. Li, L. Xu, B. Xu, R.L. Gao, Preclinical evaluation of a novel sirolimus-eluting iron bioresorbable coronary scaffold in porcine coronary artery at 6 months, JACC Cardiovasc. Interv. 12 (2019) 245–255.

[13] P. Rippstein, M.K. Black, M. Boivin, J.P. Veinot, X. Ma, Y.X. Chen, P. Human, P. Zilla, E.R. O'Brien, Comparison of processing and sectioning methodologies for arteries containing metallic stents, J. Histochem. Cytochem. 54 (2006) 673–681.

[14] International organization for standardization, Iso 10993-6, Biological Evaluation of Medical Devices; Part 6: Tests for Local Effects after Implantation, international organization for standardization: Vernier, switzerland, 2016.

[15] W.H. De Jong, J. Eelco Bergsma, J.E. Robinson, R.R. Bos, Tissue response to partially in vitro predegraded poly-l-lactide implants, Biomaterials 26 (2005) 1781–1791.

[16] S. Nakatani, M. Nishino, M. Taniike, N. Makino, H. Kato, Y. Egami, R. Shutta, J. Tanouchi, Y. Yamada, Initial findings of impact of strut width on stent coverage and apposition of sirolimus-eluting stents assessed by optical coherence tomography, Cathet. Cardiovasc. Interv. 81 (2013) 776–781.

[17] G. Nakazawa, A.V. Finn, M. Vorpahl, E.R. Ladich, F.D. Kolodgie, R. Virmani, Coronary responses and differential mechanisms of late stent thrombosis attributed to first-generation sirolimus- and paclitaxel-eluting stents, J. Am. Coll. Cardiol. 57 (2011) 390–398.

[18] G. Niccoli, R.A. Montone, G. Ferrante, F. Crea, The evolving role of inflammatory biomarkers in risk assessment after stent implantation, J. Am. Coll. Cardiol. 56 (2010) 1783–1793.

[19] M. Haude, H. Ince, A. Abizaid, R. Toelg, P.A. Lemos, C. von Birgelen, E. H. Christiansen, W. Wijns, F.J. Neumann, C. Kaiser, E. Eeckhout, S.T. Lim, J. Escaned, Y. Onuma, H.M. Garcia-Garcia, R. Waksman, Sustained safety and performance of the second-generation drug-eluting absorbable metal scaffold in patients with de novo coronary lesions: 12-month clinical results and angiographic findings of the biosolve-ii first-in-man trial, Eur. Heart J. 37 (2016) 2701–2709.

[20] Y.F. Zheng, X.N. Gu, F. Witte, Biodegradable metals, Mater. Sci. Eng. R Rep. 77 (2014) 1–34.

[21] E. Wittchow, N. Adden, J. Riedmuller, C. Savard, R. Waksman, M. Braune, Bioresorbable drug-eluting magnesium-alloy scaffold: design and feasibility in a porcine coronary model, EuroIntervention 8 (2013) 1441–1450.

[22] J.G. Speight, Lange's Handbook of Chemistry, sixteenth ed., Mcgraw-hill companies, New york, ny, 2004, pp. 1333–1342.

[23] D.R. Lide, Handbook of Chemistry and Physics, 84th edition, Crc press, Boca raton, fl, 2003, p. 688.

[24] L. Wang, G.H. Nancollas, Calcium orthophosphates: crystallization and dissolution, Chem. Rev. 108 (2008) 4628–4669.

[25] A. Aspelund, M.R. Robciuc, S. Karaman, T. Makinen, K. Alitalo, Lymphatic system in cardiovascular medicine, Circ. Res. 118 (2016) 515–530.

[26] F.D. Birkhauser, U.E. Studer, J.M. Froehlich, M. Triantafyllou, L.J. Bains, G. Petralia, P. Vermathen, A. Fleischmann, H.C. Thoeny, Combined ultrasmall superparamagnetic particles of iron oxide-enhanced and diffusion-weighted magnetic resonance imaging facilitates detection of metastases in normal-sized pelvic lymph nodes of patients with bladder and prostate cancer, Eur. Urol. 64 (2013) 953–960.

[27] L. Pedro, Q. Harmer, E. Mayes, J.D. Shields, Impact of locally administered carboxydextran-coated super-paramagnetic iron nanoparticles on cellular immune function, Small 15 (2019), e1900224.

[28] Y. Qi, H. Qi, Y. He, W. Lin, P. Li, L. Qin, Y. Hu, L. Chen, Q. Liu, H. Sun, Q. Liu, G. Zhang, S. Cui, J. Hu, L. Yu, D. Zhang, J. Ding, Strategy of metal-polymer composite stent to accelerate biodegradation of iron-based biomaterials, ACS Appl. Mater. Interfaces 10 (2018) 182–192.

[29] Y. Qi, X. Li, Y. He, D. Zhang, J. Ding, Mechanism of acceleration of iron corrosion by a polylactide coating, ACS Appl. Mater. Interfaces 11 (2019) 202–218.

[30] X. Li, W. Zhang, W. Lin, H. Qiu, Y. Qi, X. Ma, H. Qi, Y. He, H. Zhang, J. Qian, G. Zhang, R. Gao, D. Zhang, J. Ding, Long-term efficacy of biodegradable metal-polymer composite stents after the first and the second implantations into porcine coronary arteries, ACS Appl. Mater. Interfaces 12 (2020) 15703–15715.

[31] W. Lin, H. Zhang, W. Zhang, H. Qi, G. Zhang, J. Qian, X. Li, L. Qin, H. Li, X. Wang, H. Qiu, X. Shi, W. Zheng, D. Zhang, R. Gao, J. Ding, In vivo degradation and endothelialization of an iron bioresorbable scaffold, Bioact Mater 6 (2021) 1028–1039.

[32] D. Shen, H. Qi, W. Lin, W. Zhang, D. Bian, X. Shi, L. Qin, G. Zhang, W. Fu, K. Dou, B. Xu, Z. Yin, J. Rao, M. Alwi, S. Wang, Y. Zheng, D. Zhang, R. Gao, Pdlla-zn-nitrided fe bioresorbable scaffold with 53-mum-thick metallic struts and tunable multistage biodegradation function, Sci. Adv. 7 (2021).